Ultra-sensitive atomic spin measurements with a nonlinear interferometer

R. J. Sewell,[1,*] M. Napolitano,[1] N. Behbood,[1]
G. Colangelo,[1] F. Martin Ciurana,[1] and M. W. Mitchell[1,2]

[1] *ICFO-Institut de Ciencies Fotoniques, Mediterranean Technology Park, 08860 Castelldefels (Barcelona), Spain*

[2] *ICREA – Institució Catalana de Recerca i Estudis Avançats, 08015 Barcelona, Spain*

(Dated: October 23, 2013)

Quantum metrology[1,2] studies and improves quantum-limited ultra-sensitive measurements. Both linear interferometers, e.g. gravitational wave observatories[3,4], and nonlinear interferometers, e.g. optical magnetometers[5–7], have been enhanced by quantum metrology. The sensitivities of nonlinear interferometers scale better with system size than even quantum-enhanced linear interferometers[8,9], so-called 'super-Heisenberg scaling', but it is actively debated whether this scaling can lead to better absolute sensitivity[10–15]. Here we demonstrate a nonlinear measurement that surpasses, through super-Heisenberg scaling, the best possible linear measurement of the same quantity. We use alignment-to-orientation conversion[16], a practical magnetometry technique[17], to make a quantum non-demolition measurement[18] of the spin alignment of a sample of ^{87}Rb atoms[19,20]. We observe absolute sensitivity 9 dB beyond the best comparable linear measurement and measurement-induced spin squeezing. The results provide insight into ultra-sensitive magnetometers and will enable a new class of ultra-sensitive instruments. Beyond magnetometry, our techniques have potential application in the detection of exotic phases in quantum lattice gases[21,22] and spinor condensates[23,24].

Optical magnetometers[17] (OMs) achieve unsurpassed magnetic sensitivities[25] using optical interferometry to detect atomic spin precession. The most sensitive OMs, including spin-exchange relaxation-free[26] and nonlinear magneto-optic rotation[27] instruments, operate in high-N_{L} regimes with strong nonlinear effects, as do interferometers employing Bose-Einstein condensates[5,28].

A nonlinear interferometer experiences phase shifts ϕ that depend on N_{L}, the particle number (here the number of photons)[29], e.g. $\phi = \kappa N_{\mathrm{L}} \mathcal{Y}$ for a Kerr-type nonlinearity $\mathcal{Y}$, where κ is a coupling constant. This implies a sensitivity $\Delta\mathcal{Y} \geq (\kappa N_{\mathrm{L}})^{-1}\Delta\phi$, and if the nonlinear mechanism does not add noise beyond the $\Delta\phi = N_{\mathrm{L}}^{-1/2}$ shot-noise, sensitivity $\Delta\mathcal{Y} \propto N_{\mathrm{L}}^{-3/2}$ even without entanglement. Such a nonlinear system was identified in theory by Boixo et al.[11] and implemented with good agreement by Napolitano et al.[9,30]. In contrast, entanglement-enhanced linear measurement achieves at best the so-called "Heisenberg limit" $\Delta\phi = N_{\mathrm{L}}^{-1}$. The faster scaling of the nonlinear measurement suggests a decisive technological advantage for sufficiently large N_{L}. Despite this, no experiment has yet employed improved scaling to give superior absolute sensitivity, and several theoretical works[10–15] cast doubt upon this possibility for practical and/or fundamental reasons.

We study in detail the sensitivity and scaling of nonlinear Faraday rotation by alignment-to-orientation conversion (AOC)[16], recently used to generate spin-squeezing in an optical magnetometer[20]. Unlike earlier nonlinear strategies[9,11], AOC is not described by a nonlinear Hamiltonian, but rather by multiple application of a linear Hamiltonian. Via a full quantum calculation, we predict scaling $\Delta\mathcal{Y} \propto N_{\mathrm{L}}^{-3/2}$ without entanglement, which we confirm in experiment. Relative to earlier nonlinear strategies[9], AOC allows increasing N_{L} by an order of magnitude, giving 20 dB more signal and 10 dB less noise. The resulting spin alignment sensitivity surpasses by 9 dB the best possible sensitivity of a linear measurement with the same resources (photon number and allowed damage to the state). Calculations indicate that this advantage holds over all metrologically-relevant conditions. This demonstrates the practical advantage of nonlinear measurement in a quantum-limited scenario. Beyond magnetometry, quantum non-demolition measurement of spin alignment[18] has potential application in detection of exotic phases in quantum lattice gases[21,22] and spinor condensates[23,24].

We work with an ensemble of $N_{\mathrm{A}} \sim 10^6$ laser cooled ^{87}Rb atoms held in an optical dipole trap, as illustrated in Fig. 1(a) and described in detail in Ref.[31]. The atoms are prepared in the $f = 1$ hyperfine ground state, and interact dispersively with light pulses of duration τ

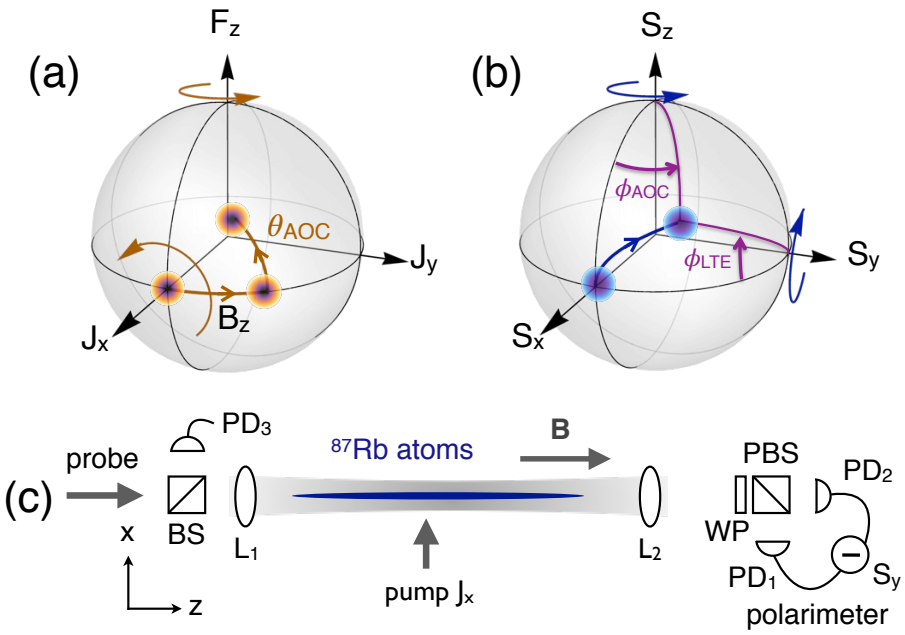

FIG. 1. Alignment–to–orientation conversion measurement of atomic spins. (a) An unknown field B_z rotates an initially J_x–polarized state in the J_x–J_y plane. The J_y component is detected using an S_x–polarized probe, which produces a rotation of J_y toward F_z by an angle $\theta_{\rm AOC} = \kappa_2 S_x/2$. (b) Simultaneously, paramagnetic Faraday rotation produces a rotation of S_x toward S_y. The net effect is a rotation $\Phi_{\rm AOC} = \kappa_1\kappa_2 N_L J_y/4$, which is observed by detecting S_y. In an alternative strategy, the linear–to–elliptical rotation of S_x towards S_z by the angle $\Phi_{LTE} = \kappa_2 J_y$ can be observed by detecting S_z. (c) Experimental geometry. Near-resonant probe pulses pass through a cold cloud of ^{87}Rb atoms and experience a Faraday rotation by an angle proportional to the on-axis collective spin F_z. Atoms are prepared in a coherent spin state J_x via optical pumping. The pulses are initially polarized with maximal Stokes operator S_x, measured at the input by photodiode (PD_3). Rotation toward S_y is detected by a balanced polarimeter consisting of a wave-plate (WP), polarizing beam-splitter (PBS), and photodiodes ($PD_{1,2}$).

via an effective Hamiltonian[32]

$$H_{\rm eff} = \kappa_1 F_z \tilde{S}_z + \kappa_2 (J_x \tilde{S}_x + J_y \tilde{S}_y) - \gamma_F \mathbf{B}\cdot\mathbf{F}, \tag{1}$$

where the coupling coefficients $\kappa_{1,2}$ are proportional to the vectorial and tensorial polarizability, respectively, and γ_F is the ground-state gyromagnetic ratio. Here $(J_x, J_y, F_z/2)$ describe the collective atomic spin, and the optical polarization is described by the pulse-

integrated Stokes operators $\int dt\, \tilde{S}_i(t) \equiv S_i$ (see Methods). J_x and J_y represent the collective spin alignment, i.e. Raman coherences between states with $\Delta m_f = 2$, and F_z describes the collective spin orientation along the quantization axis, set by the direction of propagation of the probe pulses. S_x and S_y describe linear polarizations while S_z is the degree of circular polarization, i.e., the ellipticity.

An unknown field component B_z is detected via Equation (1) through the rotation it produces on the ensemble, initially prepared in a J_x-polarized state: The $\mathbf{B}\cdot\mathbf{F}$ term rotates J_x toward J_y, making J_y an indicator of B_z[20]. In turn, J_y can be detected by measuring the polarization rotation of an input J_x-polarized optical pulse, i.e. paramagnetic Faraday rotation. This can be achieved with either a linear or a nonlinear measurement strategy, as we now describe (see Figure 1). Both strategies employ the same measurement resources, namely an S_x-polarized coherent-state probe, so that the quantum uncertainty on the input polarization angles are $\Delta S_\mathrm{y}^{(\mathrm{in})}/S_\mathrm{x} = \Delta S_\mathrm{z}^{(\mathrm{in})}/S_\mathrm{x} = N_\mathrm{L}^{-1/2}$, where N_L is the number of photons.

Linear-to-Elliptical (LTE) measurement of J_y employs the term $\kappa_2 S_\mathrm{y} J_\mathrm{y}$ to rotate the S_x-polarized probe toward S_z by a small angle $\langle\Phi_{LTE}\rangle = \kappa_2\langle J_\mathrm{y}\rangle$. S_z is directly detected, giving quantum-limited sensitivity $(\Delta J_\mathrm{y})_\mathrm{LTE} = (1/\kappa_2)(\Delta S_\mathrm{z}^{(\mathrm{in})}/S_\mathrm{x}) = (1/\kappa_2)N_\mathrm{L}^{-1/2}$, i.e., with shot-noise scaling.

AOC measurement of J_y employs H_eff twice and gives a signal nonlinear in N_L: The term $\kappa_2 S_\mathrm{x} J_\mathrm{x}$ produces a rotation of J_y toward F_z by an angle $\theta_\mathrm{AOC} = \kappa_2 S_\mathrm{x}/2$. Simultaneously, the term $\kappa_1 S_\mathrm{z} F_\mathrm{z}$ produces a rotation of S_x toward S_y by an angle $\Phi_\mathrm{AOC} = \kappa_1 F_\mathrm{z}$. The net effect is an optical rotation $\langle\Phi_\mathrm{AOC}\rangle = \kappa_1\kappa_2 N_\mathrm{L}\langle J_\mathrm{y}\rangle/4$, which is observed by detecting S_y. The quantum-limited noise of this nonlinear measurement is (see Methods)

$$(\Delta J_\mathrm{y})^2_\mathrm{AOC} = (\frac{4}{\kappa_2 N_\mathrm{L}})^2(\frac{1}{\kappa_1^2 N_\mathrm{L}} + \frac{N_\mathrm{A}}{4}) \tag{2}$$

with scaling $\Delta J_\mathrm{y} \propto N_\mathrm{L}^{-3/2}$ crossing over to $\Delta J_\mathrm{y} \propto N_\mathrm{L}^{-1}$ at large N_L.

In addition to the coherent rotations produced by H_eff, spontaneous scattering of probe photons causes two kinds of "damage" to the spin state: loss of polarization (decoherence) and added spin noise (see Methods). The trade-off between information gain and damage is what ultimately limits the sensitivity of the J_y measurement[18,32,33]. For equal N_L, the damage is the same for the LTE and AOC measurements, because they have the same initial conditions and differ only in whether S_z or S_y is detected.

From these scaling considerations, the AOC measurement should surpass the LTE mea-

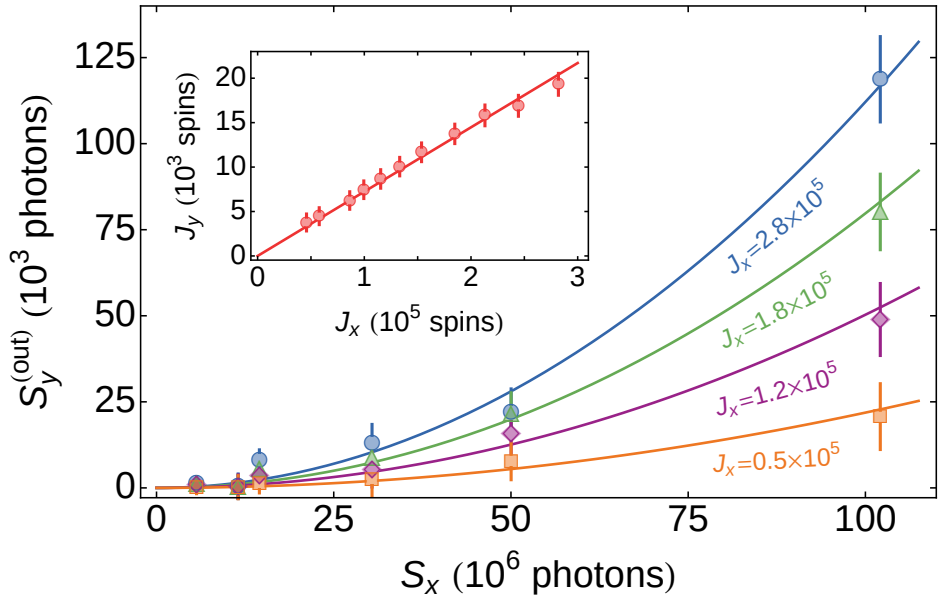

FIG. 2. Alignment-to-orientation conversion measurement of J_y. In the main frame we plot the signal $S_y^{(out)}$ of the AOC measurement as a function of S_x for various J_x. We find the measured signal J_y from fit to data using the function $S_y^{(out)} = (\kappa_1\kappa_2/2)J_y S_x^2$ (solid lines). Error bars represent $\pm 1\sigma$ statistical errors. In the inset we plot the measured J_y versus J_x. For small rotation angles $J_y \simeq 2\omega_L B_z t J_x$.

surement in sensitivity, $(\Delta J_y)_{AOC} < (\Delta J_y)_{LTE}$ for $N_L \gtrsim 16/(\kappa_1^2 N_L) + 4N_A$, but only if such a large N_L does not cause excessive scattering damage to J_y. In atomic ensembles, the achievable information/damage tradeoff is determined by the optical depth[32] (OD), which in principle can grow without bound. For high-OD ensembles the nonlinear measurement will, through advantageous scaling, surpass the best possible linear measurement of the same quantity, under the same conditions. In what follows, we demonstrate this experimentally, by comparing measured AOC sensitivity to the calculated best-possible sensitivity of the LTE measurement.

The experimental system, illustrated in Fig. 1(c), is the same as in Ref.[20], with full details given in Ref.[31]. After loading up to 6×10^5 laser–cooled atoms into a single beam optical dipole trap, we prepare a J_x-aligned coherent spin state (CSS) via optical pumping, $\langle J_x \rangle = N_A/2$. An (unknown) bias field B_z rotates the state in the J_x–J_y plane at a rate $2\omega_L$, where $\omega_L = -\gamma_F B_z$ is the Larmor frequency, to produce $\langle J_y \rangle = \sin(2\omega_L t)\langle J_x \rangle$. We probe the atoms with a sequence of 2 μs long pulses of light sent through the atoms at 5 μs

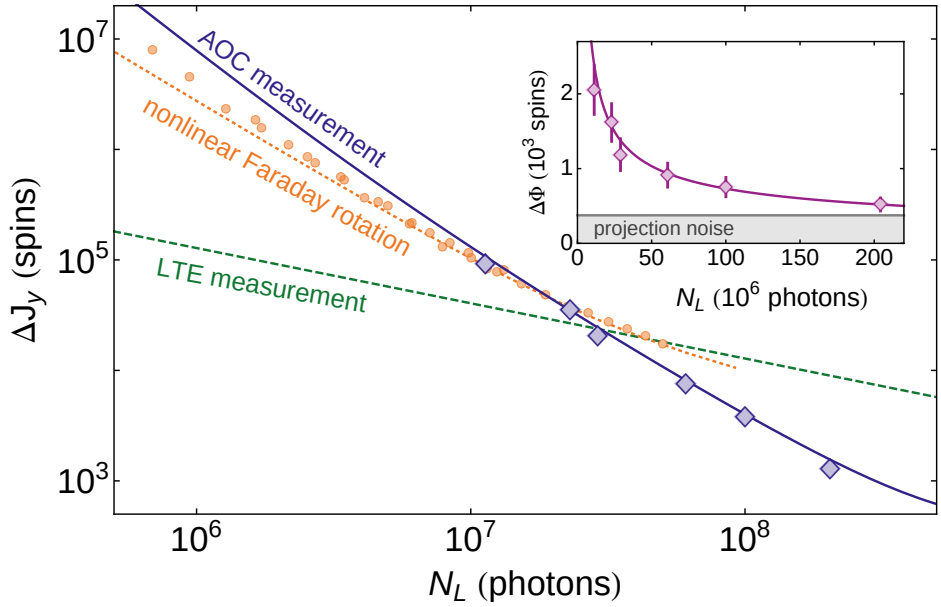

FIG. 3. Log–log plot of the uncertainty $\Delta J_{\rm y}$ of the AOC measurement versus number of photons $N_{\rm L}$. Blue diamonds indicate the measured sensitivity with no noise subtraction. Nonlinear enhanced scaling of the sensitivity is observed over more than one order of magnitude. A fit to the data yields $\Delta J_{\rm y} \propto N_{\rm L}^k$ with $k = -1.46 \pm 0.04$. The best observed sensitivity is $\Delta J_{\rm y} = 1190 \pm 90$ spins with $N_{\rm L} = 2 \times 10^8$ photons. For reference, we also plot the data (orange circles) and theory (dotted orange curve) for the measurement of $F_{\rm z}$ via nonlinear Faraday rotation reported in Napolitano et al.[9] Blue curve: theory given by Eq.(2) with no free parameters, plus the independently measured electronic noise contribution. Dashed green curve: ideal LTE measurement of $J_{\rm y}$. The nonlinear measurement sensitivity surpasses an ideal LTE measurement with $N_{\rm L} = 3 \times 10^7$ photons. Error bars for standard errors would be smaller than the symbols and are not shown. Inset: Standard deviation $\Delta\Phi$ of the AOC rotation angle scaled to have units of spins (purple diamonds). For these data $J_{\rm x} = 2.8 \times 10^5$ spins. The projection noise of the CSS is indicated by the grey line. Purple curve: theoretical prediction $\Delta\Phi = \sqrt{\cos^2\theta/\kappa_1^2 N_{\rm L} + N_{\rm A}/4}$ plus electronic noise. With $N_{\rm L} = 2 \times 10^8$ photons we observe a minimum $\Delta\Phi = 520 \pm 40$ spins with $N_{\rm L} = 2 \times 10^8$ photons. Error bars indicate $\pm 1\sigma$ standard errors.

intervals, and record $S_{\rm y}^{(\rm out)}$ with a shot–noise limited balanced polarimeter. The pulses have alternating v- and h-polarization and a detuning $\Delta/2\pi = -600$ MHz, i.e. to the red of the $F = 1 \rightarrow F' = 0$ transition on the D_2 line. The alternating polarization of the optical pulses

prevents the $J_y \rightarrow F_z$ rotation from accumulating during a multi–pulse measurement. Since the sign of the optical rotation also changes with input polarization, we make a differential measurement of J_y taking the difference between the AOC signal from a single pulse, and a baseline measurement synthesized from a pair of h– and v–polarized pulses, as described in detail in earlier works[19,20]. To study noise scaling we vary both the number of photons per pulse N_L, and the number of atoms N_A in the initial CSS.

In Fig. 2 we plot the observed signal $S_y^{(out)}$ versus S_x for various values of J_x. As expected, we observe a signal that increases quadratically with S_x. We extract $\langle J_y \rangle$ from a fit to data using the function $S_y^{(out)} = (\kappa_1 \kappa_2/2)\langle J_y \rangle S_x^2$ (solid lines in Fig. 2), where the coupling constants $\kappa_1 = 1.47 \times 10^{-7}$ rad/spin and $\kappa_2 = 7.54 \times 10^{-9}$ rad/spin are independently measured (see Methods). In the inset we plot the measured $\langle J_y \rangle$ versus $\langle J_x \rangle$. For small rotation angles $\langle J_y \rangle \simeq 2\,\omega_L t \langle J_x \rangle$, where $t = 7.5$ μs is the time between the centers of the baseline and AOC measurements. A linear fit to the data yields $B_z = 109 \pm 2$ nT.

The measured sensitivity $\Delta J_y = \Delta S_y / (\kappa_1 \kappa_2 S_x^2)$ is obtained from the measured readout variation ΔS_y and the slope $\partial \langle S_y \rangle / \partial \langle J_y \rangle = \kappa_1 \kappa_2 S_x^2$. As shown in Fig. 3, we observe nonlinear enhanced scaling $\Delta J_y \propto N_L^{-3/2}$ over more than one order of magnitude in N_L. For these data $\langle J_x \rangle = 2.8 \times 10^5$ and $\langle J_y \rangle = 1.9 \times 10^4$. The data are well described by the theoretical model of Eq. 2, plus a small offset due to electronic noise, which is independently measured (see Methods). We observe a minimum $\Delta J_y = 1190 \pm 90$ spins with $N_L = 2 \times 10^8$ photons.

The AOC measurement sensitivity crosses below the ideal LTE measurement $(\Delta J_y)_{LTE} = (1/\kappa_2) N_L^{-1/2}$ (dashed green line in Fig. 3) with $N_L = 3 \times 10^7$ photons, indicating that, for our experimental parameters, the nonlinear measurement is the superior measurement of J_y. For comparison, we also compare our measurement of the alignment J_y with the nonlinear Faraday rotation measurement of F_z reported in Napolitano et al.[9] (orange circles and dotted line in Fig. 3). We note in particular that the advantageous scaling of the current measurement extends to an order of magnitude larger N_L than reported in that work.

Projection-noise limited measurement can be used to prepare a conditional spin squeezed atomic state[34]. This is a useful metric for the measurement sensitivity since it takes into account damage done to the atomic state by the optical probe[18,35]. Here it is important to note that although the AOC signal is proportional to the atomic spin alignment J_y, quantum noise from the spin orientation F_z is mixed into the measurement[20].

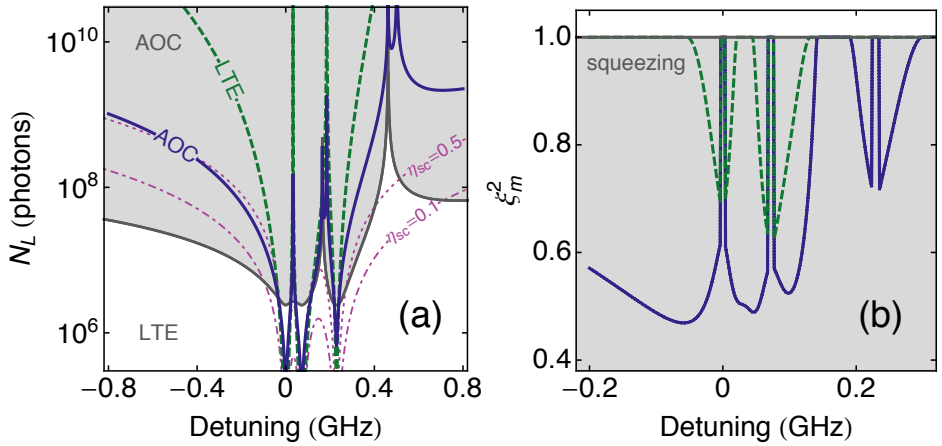

FIG. 4. Comparison of AOC (dark blue curves), and LTE (green dashed curves) measurement sensitivity. (a) Number of photons $N_{\rm L}$ needed to achieve projection noise limited sensitivity $(\Delta J_{\rm y})^2_{\rm AOC} = (\Delta J_{\rm y})^2_{\rm LTE} = N_{\rm A}/4$ as a function of detuning Δ. The gray line indicates $(\Delta J_{\rm y})^2_{\rm AOC} = (\Delta J_{\rm y})^2_{\rm LTE}$, so that the AOC (LTE) strategy is more sensitive in the shaded (white) region. Magenta curves: damage $\eta_{\rm sc} = 0.1$ (dot–dashed) and 0.5 (dotted) to the atomic state due to spontaneous emission. (b) Estimated metrologically significant spin squeezing $\xi^2_{\rm m}$, optimized as a function of $N_{\rm L}$, versus probe detuning.

Scaled to have units of spins, the Faraday rotation signal from the AOC measurement is $\Phi \equiv (\cos\theta/\kappa_1 S_{\rm x}) S_{\rm y}^{\rm (out)} = (\cos\theta/\kappa_1 S_{\rm x}) S_{\rm y}^{\rm (in)} + K_\theta$, which describes a quantum nondemolition measurement[18] of the mixed alignment–orientation variable $K_\theta \equiv F_{\rm z}\cos\theta + J_{\rm y}\sin\theta$, where $\tan\theta \equiv \kappa_2 S_{\rm x}/2$ (see Methods). This is the variable that should be squeezed to enhance the sensitivity of the AOC measurement. In the inset of Fig. 3 we plot the RMS uncertainty $\Delta\Phi = \sqrt{\cos^2\theta/\kappa_1^2 N_{\rm L} + N_{\rm A}/4}$ as a function of photon number. We observe a minimum $\Delta\Phi = 520 \pm 40$ spins, with $N_{\rm L} = 2\times10^8$ and $J_{\rm x} = 2.8\times10^5$, corresponding to a measurement sensitivity of of $\Delta\Phi_0 \equiv \sqrt{\cos^2\theta/\kappa_1^2 N_{\rm L}} = 360 \pm 50$ spins. With these parameters we observe a conditional noise 2.3 ± 0.5 dB below the projection noise limit $(\Delta K_\theta)^2 = J_{\rm x}/2$ and $\xi^2_{\rm m} = 0.73\pm0.09$, or 1.4 ± 0.5 dB of metrologically significant spin squeezing according to the Wineland criterion[35]. The measurement sensitivity and spin squeezing of the K_θ variable are comparable to state-of-the-art single-pass measurements[20,36,37]. We note also that for our experimental parameters, LTE would not induce spin squeezing (see Methods).

The experiment shows AOC surpassing LTE through improved scaling at the specific de-

tuning of $\Delta/2\pi = -600$ MHz. It is important to ask whether this advantage persists under other measurement conditions. A good metric for the optimum measurement is the number of photons $N_{\rm L}$ required to achieve a given sensitivity (see Methods). In Fig. 4(a) we plot the calculated $N_{\rm L}$ required to reach projection noise limited sensitivity for the two measurement strategies, i.e. $(\Delta J_{\rm y})^2_{\rm AOC} = (\Delta J_{\rm y})^2_{\rm LTE} = N_{\rm A}/4$ for our experimental parameters. For comparison, we also plot curves showing the damage $\eta_{\rm sc}$ to the atomic state due to spontaneous emission (see Methods). We see that the AOC strategy is more sensitive except close to the atomic resonances where the probability of scattering a photon is large. An alternate metric is to optimize the metrologically significant squeezing $\xi^2_{\rm m}$ as a function of $N_{\rm L}$ for a given detuning. In Fig. 4(b) we show $\xi^2_{\rm m}$ versus detuning. We estimate optimum squeezing achieved by the AOC (LTE) strategy is $\xi^2_{\rm m} = 0.47$ (0.63) at a detuning of $\Delta/2\pi = -59$ MHz (+77MHz).

We conclude that: 1) For nearly all probe frequencies, if $N_{\rm L}$ is chosen to give projection-noise sensitivity for LTE, then AOC at the same frequency and $N_{\rm L}$ gives better sensitivity. The exception is probing very near an absorption resonance, which induces a large decoherence in the atomic state. 2) Considering as a figure of merit the achievable spin squeezing, or equivalently the magnetometric sensitivity of a Ramsey sequence employing these measurements[20], the global optimum including choice of measurement is AOC at a detuning of -59 MHz, with $N_{\rm L} = 5.4 \times 10^6$ photons. In this practical metrological sense, the nonlinear measurement is unambiguously superior. Although the AOC and LTE compared here use coherent states as inputs, the same conclusion is expected when non-classical probe states are used: for both measurements the optical rotation sensitivity $\Delta S^{\rm (in)}_{\rm y,z}/S_{\rm x}$ can be enhanced in the same way by squeezing[6] and other techniques[33].

---

* robert.sewell@icfo.es

[1] V. Giovannetti, S. Lloyd, L. Maccone, *Science* **306**, 1330 (2004).

[2] V. Giovannetti, S. Lloyd, L. Maccone, *Nat. Photon.* **5**, 222 (2011).

[3] C. M. Caves, *Phys. Rev. D* **23**, 1693 (1981).

[4] The LIGO Scientific Collaboration, *Nat. Phys.* **7**, 962 (2011).

[5] B. Luecke, *et al.*, *Science* **334**, 773 (2011).

[6] F. Wolfgramm, *et al.*, *Phys. Rev. Lett.* **105**, 053601 (2010).

[7] T. Horrom, R. Singh, J. P. Dowling, E. E. Mikhailov, *Phys. Rev. A* **86**, 023803 (2012).

[8] S. Boixo, *et al.*, *Phys. Rev. A* **77**, 012317 (2008).

[9] M. Napolitano, *et al.*, *Nature* **471**, 486 (2011).

[10] A. M. Rey, L. Jiang, M. D. Lukin, *Phys. Rev. A* **76**, 053617 (2007).

[11] S. Boixo, *et al.*, *Phys. Rev. Lett.* **101**, 040403 (2008).

[12] J. Javanainen, H. Chen, *Phys. Rev. A* **85**, 063605 (2012).

[13] M. Zwierz, C. Pérez-Delgado, P. Kok, *Phys Rev Lett* **105**, 180402 (2010).

[14] R. Demkowicz-Dobrzanski, J. Kolodynski, M. Guta, *Nat. Comm.* **3**, 1063 (2012).

[15] M. J. W. Hall, H. M. Wiseman, *Physical Review X* **2**, 041006 (2012).

[16] D. Budker, D. F. Kimball, S. M. Rochester, V. V. Yashchuk, *Phys. Rev. Lett.* **85**, 2088 (2000).

[17] D. Budker, M. Romalis, *Nat. Phys.* **3**, 227 (2007).

[18] R. J. Sewell, M. Napolitano, N. Behbood, G. Colangelo, M. W. Mitchell, *Nat. Photon.* **7**, 517 (2013).

[19] M. Koschorreck, M. Napolitano, B. Dubost, M. W. Mitchell, *Phys. Rev. Lett.* **105**, 093602 (2010).

[20] R. J. Sewell, *et al.*, *Phys. Rev. Lett.* **109**, 253605 (2012).

[21] K. Eckert, *et al.*, *Nat. Phys.* **4**, 50 (2008).

[22] P. Hauke, R. J. Sewell, M. W. Mitchell, M. Lewenstein, *Phys. Rev. A* **87**, 021601 (2013).

[23] K. Eckert, L. Zawitkowski, A. Sanpera, M. Lewenstein, E. S. Polzik, *Phys. Rev. Lett.* **98**, 100404 (2007).

[24] C. D. Hamley, C. S. Gerving, T. M. Hoang, E. M. Bookjans, M. S. Chapman, *Nat. Phys.* **8**, 305 (2012).

[25] I. K. Kominis, T. W. Kornack, J. C. Allred, M. V. Romalis, *Nature* **422**, 596 (2003).

[26] J. C. Allred, R. N. Lyman, T. W. Kornack, M. V. Romalis, *Phys. Rev. Lett.* **89**, 130801 (2002).

[27] D. Budker, D. F. Kimball, S. M. Rochester, V. V. Yashchuk, M. Zolotorev, *Phys. Rev. A* **62**, 043403 (2000).

[28] J. Esteve, C. Gross, A. Weller, S. Giovanazzi, M. K. Oberthaler, *Nature* **455**, 1216 (2008).

[29] A. Luis, *Phys. Lett. A* **329**, 8 (2004).

[30] M. Napolitano, M. W. Mitchell, *New J. Phys.* **12**, 093016 (2010).

[31] M. Kubasik, *et al.*, *Phys. Rev. A* **79**, 043815 (2009).

[32] S. R. de Echaniz, *et al.*, *J. Opt. B* **7**, S548 (2005).

[33] F. Wolfgramm, C. Vitelli, F. A. Beduini, N. Godbout, M. W. Mitchell, *Nat. Photon.* **7**, 28 (2013).

[34] A. Kuzmich, N. P. Bigelow, L. Mandel, *Europhys. Lett.* **42**, 481 (1998).

[35] D. J. Wineland, J. J. Bollinger, W. M. Itano, F. L. Moore, D. J. Heinzen, *Phys. Rev. A* **46**, R6797 (1992).

[36] J. Appel, *et al.*, *Proc. Natl. Acad. Sci. U.S.A.* **106**, 10960 (2009).

[37] M. Koschorreck, M. Napolitano, B. Dubost, M. W. Mitchell, *Phys. Rev. Lett.* **104**, 093602 (2010).

Acknowledgments We thank I. Walmsely, A. Datta and J. Nunn for useful discussions, and M. Koschorreck and R. P. Anderson for helpful comments. This work was supported by the Spanish Ministerio de Economía y Competitividad under the project Magnetometria ultra-precisa basada en optica quantica (MAGO) (Ref. FIS2011-23520), by the European Research Council under the project Atomic Quantum Metrology (AQUMET) and by Fundació Privada CELLEX Barcelona.

SUPPLEMENTARY INFORMATION

Atom–light interaction.

As described in Ref.[32] the light pulses and atoms interact by the effective Hamiltonian

$$H_{\rm eff} = \kappa_1 F_{\rm z} \tilde{S}_z(t) + \kappa_2 [J_{\rm x} \tilde{S}_x(t) + J_{\rm y} \tilde{S}_y(t)], \tag{3}$$

plus higher-order terms describing fast electronic nonlinearities[30]. Here $\kappa_{1,2}$ are coupling constants that depend on the beam geometry, excited-state linewidth, laser detuning, and the hyperfine structure of the atom, and the light is described by the time-resolved Stokes operator $\tilde{\mathbf{S}}(t)$, defined as $\tilde{S}_i \equiv \frac{1}{2}(\mathcal{E}_+^{(+)}, \mathcal{E}_-^{(+)})\sigma_i(\mathcal{E}_+^{(+)}, \mathcal{E}_-^{(+)})^T$, where the σ_i are the Pauli matrices and $\mathcal{E}_\pm^{(+)}(t)$ are the positive frequency parts of quantized fields for the circular plus/minus polarizations. The pulse-averaged Stokes operators are $S_i \equiv \int dt\, \tilde{S}_i(t)$ so that $S_i = \frac{1}{2}(a_+^\dagger, a_-^\dagger)\sigma_i(a_+, a_-)^T$, where $a_\pm$ are operators for the temporal mode of the pulse[20]. In all scenarios of interest $|\langle J_{\rm x}\rangle| \approx N_{\rm A}/2 \gg |\langle J_{\rm y}\rangle|, |\langle F_{\rm z}\rangle|$, and we use input $S_{\rm x}$-polarized light

pulses, $|\langle S_{\rm x}^{(\rm in)}\rangle| = N_{\rm L}/2$, and detect the output $S_{\rm y}^{(\rm out)}$ component of the optical polarization.

The atomic spin ensemble is characterized by the operators $F_{\rm z} \equiv \sum_i^{N_{\rm A}} f_{\rm z}^{(i)}$, describing the collective spin orientation, and $J_{\rm x,y} \equiv \sum_i^{N_{\rm A}} \hat{\jmath}_{\rm x,y}^{(i)}$, describing the collective spin alignment, where $\hat{\jmath}_{\rm x} \equiv (f_{\rm x}^2 - f_{\rm y}^2)/2$ and $\hat{\jmath}_{\rm y} \equiv (f_{\rm x}f_{\rm y} + f_{\rm y}f_{\rm x})/2$ describe single-atom Raman coherences, i.e., coherences between states with $\Delta m_f = 2$. Here $\mathbf{f}^{(i)}$ is the total spin of the i'th atom. For $f = 1$, these obey commutation relations $[J_{\rm x}, J_{\rm y}] = i(F_{\rm z}/2)$ and cyclic permutations.

Using Eq. 3 in the Heisenberg equations of motion and integrating over the duration of a single light pulse[20], we find the detected outputs to second order in $S_{\rm x}$

$$S_{\rm z}^{(\rm out)} = S_{\rm z}^{(\rm in)} + \kappa_2 S_{\rm y} J_{\rm x} - \kappa_2 S_{\rm x} J_{\rm y} \tag{4}$$

$$S_{\rm y}^{(\rm out)} = S_{\rm y}^{(\rm in)} + \kappa_1 S_{\rm x} F_{\rm z} + \frac{\kappa_1\kappa_2}{2} S_{\rm x}^2 J_{\rm y}, \tag{5}$$

plus small terms.

Measurement sensitivity.

Both AOC and LTE measurements have the same input state, with $S_{\rm x} \equiv \langle S_{\rm x}^{(\rm in)}\rangle = N_{\rm L}/2$, $\langle J_{\rm x}\rangle = N_{\rm A}/2$, $\langle F_{\rm z}\rangle = 0$, $(\Delta S_{\rm y}^{(\rm in)})^2 = N_{\rm L}/4$, $(\Delta F_{\rm z}^{(\rm in)})^2 = (\Delta J_{\rm y}^{(\rm in)})^2 = N_{\rm A}/4$ and uncorrelated $S_{\rm x}, S_{\rm y}, S_{\rm z}, F_{\rm z}$, and $J_{\rm y}$. The LTE measurement detects $S_{\rm z}$, with signal $\langle S_{\rm z}^{(\rm out)}\rangle = -\kappa_2 S_{\rm x}\langle J_{\rm y}\rangle$. The detected $S_{\rm z}$ variance, referred to the input, i.e. to $J_{\rm y}$, is

$$(\Delta J_{\rm y})^2 = \frac{(\Delta S_{\rm z}^{(\rm out)})^2}{|\partial\langle S_{\rm z}^{(\rm out)}\rangle/\partial\langle J_{\rm y}\rangle|^2} \tag{6}$$

$$= \frac{1}{\kappa_2^2 N_{\rm L}} + \frac{N_{\rm A}^2}{4N_{\rm L}} + \frac{N_{\rm A}}{4} \tag{7}$$

and shows shot-noise scaling. The first two terms are readout noise and last is the variance of $J_{\rm y}$, i.e., the signal variance. In the experiment $(\kappa_2 N_{\rm A})^2/4 \sim 10^{-3}$ so the second term is negligible. We note that other measurement strategies using the same term in the Hamiltonian are possible, e.g. probing with $S_{\rm z}$-polarized light and reading out the rotation of $S_{\rm z}$ into $S_{\rm y}$, but lead to the same measurement sensitivity.

The AOC measurement detects $S_{\rm y}$, with signal $\langle S_{\rm y}^{(\rm out)}\rangle = (\kappa_1\kappa_2 S_{\rm x}^2/2)\langle J_{\rm y}\rangle$ and variance $(\Delta S_{\rm y}^{(\rm out)})^2 = (\Delta S_{\rm y}^{(\rm in)})^2 + (\kappa_1^2 S_{\rm x}^2)(\Delta F_{\rm z}^{(\rm in)})^2 + (\kappa_1^2\kappa_2^2 S_{\rm x}^4/4)(\Delta J_{\rm y}^{(\rm in)})^2$. Referred to the input, this

is

$$(\Delta J_{\rm y})^2 = \frac{(\Delta S_{\rm y}^{(\rm out)})^2}{|\partial\langle S_{\rm y}^{(\rm out)}\rangle/\partial\langle J_{\rm y}\rangle|^2} \tag{8}$$

$$= \frac{16}{\kappa_1^2\kappa_2^2 N_{\rm L}^3} + \frac{4N_{\rm A}}{\kappa_2^2 N_{\rm L}^2} + \frac{N_{\rm A}}{4}, \tag{9}$$

where again the last term is the signal variance.

In contrast, previous work[9] used short, intense pulses to access a nonlinear term in the effective Hamiltonian $\kappa_{\rm NL} S_0 S_{\rm z} F_{\rm z}$. The coupling $\kappa_{\rm NL}$ is proportional to the Kerr nonlinear polarizability and $S_0 \equiv N_{\rm L}/2$ (so that $S_0 = S_{\rm x}$ for the input polarization used). This gives sensitivity $\Delta F_{\rm z} = \Delta S_{\rm z}^{(\rm in)}/(\kappa_{\rm NL} S_{\rm x}^2)$ and $\Delta F_{\rm z} \propto N_{\rm L}^{-3/2}$ scaling.

Electronic & technical noise.

The measured electronic noise of the detector referred to the interferometer input was EN $= 9.2 \times 10^5$ photons. This contributes a term EN $\times\, 64/(\kappa_1^2\kappa_2^2 N_{\rm L}^4)$ to Eq.(2), which is included in the blue curve plotted in Fig. 3. Technical noise contributions from both the atomic and light variables were negligible in this experiment.

Atom number.

We vary the number of atoms, $N_{\rm A}$, used in the experiment from 3.9×10^4 to 8.5×10^5 by switching off the optical dipole trap for 100 μs after each measurement, which reduces the atom number by $\sim 15\,\%$, and repeating the sequence $P = 20$ times per trap loading cycle. At the end of each cycle the measurement is repeated without atoms in the trap. To collect statistics, the entire cycle is repeated $M = 1090$ times. We then change the mean photon number $N_{\rm L}$ used in the probe pulses and repeat the entire experiment. This allows us to collect data with $N_{\rm L}$ varying from 10^7 to 2×10^8.

We measure the number of atoms via dispersive atom-number measurement (DANM) by probing the $J_{\rm x}$-polarized state with an $S_{\rm z}$-polarized pulse $\langle S_{\rm z}^{(\rm in)}\rangle = N/2$. This measurement is made using an auxiliary probe beam focused to a waist of 50 μm. This gives an optical rotation $\langle S_{\rm y}\rangle^{(\rm out)} = \kappa_2^{(\rm aux)}(N_{\rm L} N_{\rm A}/4)$, where $\kappa_2^{(\rm aux)} = 0.9 \times 10^{-7}$ radians per spin. The measurement is made with a train of μs pulses of circularly polarized light with 10^6 photons/pulse at a detuning of 190 MHz to the red of the $f = 1 \rightarrow f' = 0$ transition.

Calibration of dispersive spin measurements.

Both the AOC measurement and the DANM are calibrated against a measurement of the atom number made by absorption imaging, as described in Ref.[37]. For the AOC measurements $\kappa_1 = 1.47 \times 10^{-7}$ radians per spin, from which we calculate $\kappa_2 = 7.54 \times 10^{-9}$ radians per spin. To account for the spatial variation in the coupling between the probe beam and the trapped atoms, we define an effective total spin such that the parametric Faraday rotation signal is proportional to the collective spin, and the expected variance of the measurement variable is $(\Delta K_\theta)^2 = N_\mathrm{A}/4$[20].

Differential measurement.

Our experimental data comes in the form of sets of AOC measurement outcomes $\phi_{i,p} = \{\phi_i^{(m)}\}_p$, where i labels the pulses sent through the atoms after each state preparation, p labels the $P = 20$ independent state preparations per trap loading cycle, and m labels the $M = 1090$ repetitions of the entire sequence. Since the sign of the rotation changes with the input probe polarisation, we make a differential measurement of ϕ comparing the signal from a single-pulse AOC measurement to a baseline measurement synthesized from two sequential pulses, as described in detail in Refs.[19,20]. The average signal is then $\phi_{j,p} = \frac{1}{M}\sum_{m=1}^{k} |\frac{1}{2}(\phi_i^{(m)} - \phi_{i+1}^{(m)}) - \phi_j^{(m)}|$.

Conditional noise reduction & spin squeezing.

We note that Eq.(5) describes a quantum non-demolition measurement[18], which induces conditional spin squeezing of the mixed alignment-orientation variable $K_\theta \equiv \cos\theta F_\mathrm{z} + \sin\theta J_\mathrm{y}$, with $\theta = \arctan(\kappa_2 S_\mathrm{x}/2)$. The measurement-induced noise reduction is quantified by the conditional variance $\mathrm{var}(K_\theta|\Phi_1) = \mathrm{var}(\Phi_2 - \chi\Phi_1) - \mathrm{var}(\Phi_\mathrm{RO})$, where $\chi \equiv \mathrm{cov}(\Phi_1, \Phi_2)/\mathrm{var}(\Phi_1) > 0$ describes the correlation between Φ_1 and Φ_2, and Φ_1 is a baseline measurement as described above. We quantify spin squeezing by the Wineland criterion[35], which accounts for both the noise and the coherence of the post-measurement state: if $\xi_\mathrm{m}^2 \equiv (\Delta K_\theta)^2 J_\mathrm{x}/2|J_\mathrm{x}^{(\mathrm{out})}|^2$, where $J_\mathrm{x}^{(\mathrm{out})} = (1-\eta_\mathrm{sc})(1-\eta_\mathrm{dep})J_\mathrm{x}$ is the amplitude of the CSS after the measurement, then $\xi_\mathrm{m}^2 < 1$ indicates metrological advantage. Depolarization due to probe scattering and field inhomogeneities are $\eta_\mathrm{sc} = 0.093$ and $\eta_\mathrm{dep} = 0.034$, respectively.[20]

Dependence on detuning and optical depth.

The detuning dependence of the coupling constants κ_1 and κ_2 of Eq.(1) is given by

$$\kappa_1 = \frac{\sigma_0}{A}\frac{\Gamma}{16}\left(-4\delta_0(\Delta) - 5\delta_1(\Delta) + 5\delta_2(\Delta)\right) \tag{10}$$

$$\kappa_2 = \frac{\sigma_0}{A}\frac{\Gamma}{16}\left(4\delta_0(\Delta) - 5\delta_1(\Delta) + \delta_2(\Delta)\right) \tag{11}$$

where $\delta_i(\Delta) \equiv 1/\sqrt{\Gamma^2 + (\Delta - \Delta_i)^2}$, Δ_i is the detuning from resonance with the $F = 1 \rightarrow F' = i$ transition on the ^{87}Rb D_2 line, $\Gamma/2\pi = 6.1$ MHz is the natural linewidth of the transition, Δ is measured from the $F = 1 \rightarrow F' = 0$ transition, $\sigma_0 \equiv \lambda^2/\pi$ and $A = 4.1 \times 10^{-9}\,\mathrm{m}^2$ is the effective atom-light interaction area. Note that for large detuning, i.e. $\Delta \gg \Gamma$, $\kappa_1 \propto 1/\Delta$ and $\kappa_2 \propto 1/\Delta^2$.

At any detuning, the measurement sensitivity can be improved by increasing the number of photons N_L used in the measurement. Note, however, that increasing N_L also increases the damage $\eta_\mathrm{sc} = k(\Delta)\eta_\gamma(\Delta)N_\mathrm{L}$ done to the atomic state we are trying to measure due to probe scattering, where $\eta_\gamma(\Delta)$ is the probability of scattering a single photon:

$$\eta_\gamma = \frac{\sigma_0}{A}\frac{\Gamma^2}{64}\left(4\delta_0(\Delta)^2 + 5\delta_1(\Delta)^2 + 7\delta_2(\Delta)^2\right) \tag{12}$$

which also scales as $\eta_\gamma \propto 1/\Delta^2$ for large detuning. $k(\Delta)$ is a correction factor that accounts for the fact that a fraction of the scattering events leave the state unchanged. A good metric to compare measurement strategies is the number of photons N_L required to achieve a given sensitivity. This will minimize damage to the atomic state independently of the correction factor $k(\Delta)$. For our calculations we set $k(\Delta) = 0.4$, which predicts our measurements at large detuning

An estimate for the quantum noise reduction that can be achieved in a single-pass measurement, valid for $\eta_\mathrm{sc} \ll 1$, is given by

$$\xi^2 = \frac{1}{1+\zeta} + 2\eta_\mathrm{sc} \tag{13}$$

where ζ is the signal-to-noise ratio of the measurement, i.e. the ratio of atomic quantum noise to light shot noise in the measured variance $(\Delta S_\mathrm{y}^{(\mathrm{out})})^2$. For the two strategies considered here,

$$\zeta_\mathrm{AOC} = \frac{\kappa_1^2 N_\mathrm{L} N_\mathrm{A}}{4}\left(1 + \frac{\kappa_2^2 N_\mathrm{L}^2}{16}\right) \quad \text{and} \tag{14}$$

$$\zeta_\mathrm{LTE} = \frac{\kappa_1^2 N_\mathrm{L} N_\mathrm{A}}{4}. \tag{15}$$

Metrologically significant squeezing is then given by

$$\xi_{\rm m}^2 = \xi^2/(1-\eta_{\rm sc})^2. \tag{16}$$